

In the format provided by the authors and unedited.

High aspect ratio nanomaterials enable delivery of functional genetic material without DNA integration in mature plants

Gozde S. Demirer¹, Huan Zhang¹, Juliana L. Matos^{2,3}, Natalie S. Goh¹, Francis J. Cunningham¹, Younghun Sung¹, Roger Chang¹, Abhishek J. Aditham¹, Linda Chio¹, Myeong-Je Cho³, Brian Staskawicz^{2,3} and Markita P. Landry^{1,3,4,5*}

¹Department of Chemical and Biomolecular Engineering, University of California, Berkeley, CA, USA. ²Department of Plant and Microbial Biology, University of California, Berkeley, CA, USA. ³Innovative Genomics Institute (IGI), Berkeley, CA, USA. ⁴California Institute for Quantitative Biosciences, QB3, University of California, Berkeley, CA, USA. ⁵Chan-Zuckerberg Biohub, San Francisco, CA, USA. *e-mail: landry@berkeley.edu

SUPPLEMENTARY INFORMATION

Plant growth. Italian arugula (*Eruca sativa*) seeds purchased from Renee's Garden were germinated in SunGro Sunshine LC1 Grower soil mix by planting the seeds half an inch deep into the soil of a standard propagation liner tray (Nursery Supplies). The germinated plants were then moved to a Hydrofarm LED growth chamber (12h light at ~22°C / 12h dark at 18°C). Plants were allowed to mature to 3-4 weeks of age within the chamber before experimental use. Wild type *Nb* and transgenic mGFP5 *Nb* seeds obtained from the Staskawicz Lab, UC Berkeley, were germinated and grown in SunGro Sunshine LC1 Grower soil mix for four weeks before experimental in a growth chamber, 12-hour light at 24°C: 12-hour dark at 18°C cycle. Spring wheat (*Triticum aestivum* L., cv. Fielder) were grown in Supersoil (Rod McClellan Co., South San Francisco, CA, USA) in a Conviron growth chamber with 60% relative humidity, 18-hour light at 24°C: 8-hour dark at 18°C cycle, and 3-4-week-old plants were used for experiments. Cotton seedlings were purchased from Cottonman.com and allowed to mature within the Hydrofarm LED growth chamber (12h light at ~22°C / 12h dark at 18°C). All experiments (except gene gun) were done with intact leaves attached to plants, where plants were incubated in the growth chamber until the time of data collection.

Single molecule TIRF to image DNA protection by SWCNTs. The sequence of DNA used for this assay is the same as that used in co-localization experiments, (GT)₁₅. While Cy3 was used for co-localization assays in planta, the Cy5 fluorophore was selected for the TIRF assay due to lower levels of background noise in the collection region. 10 μM 3' labelled Cy5 DNA was added to an equal mass of HiPCO SWCNT. The suspension and clearing of unbound DNA followed the same protocol as described in SDS-CNT, ssDNA-CNT and Cy3-DNA-CNT preparation. The positive control comprised of 5' labelled biotin with a Cy5 fluorophore on the 3' end.

6-channel μ -slides (ibidi, μ -Slide VI 0.5 Glass Bottom) were used for single-molecule TIRF microscopy. The slides were initially washed by pipetting 100 μ L of 100 mM NaCl solutions in nuclease-free water filtered with a sterile 0.2 μ m syringe filter into one reservoir and removing 60 μ L the other end, leaving just enough solution to fully wet the channel. Each subsequent step involved depositing the desired solution volume into the reservoir and removing the equivalent volume from the other end of the channel. 50 μ L of 0.25 mg/mL BSA-Biotin was added to coat the surface of the glass slide for 5 minutes. Next, 50 μ L of 0.05 mg/mL NeutrAvidin was added, followed by 50 μ L of 1.0 mg/L DNA-loaded SWCNT. For the positive control, 50 μ L of 100 pM biotinylated Cy5-DNA was added in place of DNA-loaded SWCNT. The addition of each component comprised of a 5-minute incubation period, followed by gently flushing the channel with 50 μ L of NaCl solution to remove unbound entities. Each channel was exposed to 50 μ L of 2.8 U/ μ L S1 Nuclease for 30 minutes at room temperature. The reaction was stopped by rinsing the channel with 1 mM ATP solution to inactivate the nuclease. To minimize disturbance of bound DNA or DNA-SWCNT, no imaging buffer was used; each field of view obtained was ensured to not have been imaged previously.

Following slide preparation and immobilized procedure as outlined above, we obtain a surface coverage of \sim 300-400 fluorescent molecules of DNA-loaded SWCNT for each field of view, imaged with a 642 nm laser line, collected with a 655 LP filter, with a 1000 ms exposure time and an EMCCD gain of 300 under TIRF microscopy (Zeiss ELYRA PS.1).

Chloroplast extraction and SWCNT internalization imaging. Chloroplasts were extracted from 4-weeks old intact wild type Nb leaves in a sucrose buffer: 28 mM Na_2HPO_4 , 22 mM KH_2PO_4 , 2.5 mM MgCl_2 , 400 mM sucrose and 10 mM KCl at pH=7.3. All buffers and materials were previously cooled to 4°C and all centrifugation steps were performed at 4°C. Central veins of Nb leaves were removed with a sharp razor blade and leaves were grounded in food

processor without the buffer. 5 grams of ground leaves were added to 40 mL cold sucrose buffer and homogenized in mortar and pestle. Ground liquid was poured over 4 layers of cheesecloth and centrifuged at 4000 rpm for 20 min. Supernatant was discarded and the crude chloroplast pellet was resuspended in 5 mL cold sucrose buffer. The solution was centrifuged again at 4000 rpm for 20 min, and the pellet was resuspended in 5 mL cold sucrose buffer. In 2 separate 15 ml falcon tubes, 80%, 60%, 40% and 20% (v/v) Percoll and sucrose buffer are gently combined from bottom to top. 2.5 ml of each fraction is added starting with 80% and ~3 ml of chloroplast solution was gently added to the top of each tube. The gradients were centrifuged at 4000 rpm for 20 min and the dark chloroplast bands in the middle were gently removed with a pipette and combined. 5 mL cold sucrose buffer was added and the solution was centrifuged at 4000 rpm for 20 min. Chloroplasts were pelleted at the bottom and 3 mL sucrose buffer was added for the subsequent experiments. Keep chloroplast suspension in fridge at 4 °C and avoid exposure to light.

Cy3-DNA-SWCNT or ssDNA-SWCNT solutions (at a DNA concentration of 200 nM) were added to 100 µl of extracted chloroplasts, chloroplasts were pelleted after 4 hours of incubation at room temperature, and the supernatant solution was replaced to fresh sucrose buffer without SWCNTs prior to imaging either with fluorescence microscope for Cy3-DNA tracking or nIR microscope for SWCNT tracking in extracted chloroplasts, respectively.

Agrobacterium-mediated transformation. *Agrobacterium tumefaciens* strain GV3101 was used for genetic transformation of *Nb* and arugula leaves, and as a positive control in ddPCR experiments. To generate the *Agrobacterium*-binary construct, the DNA fragment containing 35S-GFP-NOS were excised from the plasmid 35sC4PPDKsGFPTYG with the restriction enzymes *Xho*I and *Eco*RI and cloned into an entry cloned digested with the same restriction enzymes. The 35S-GFP-NOS entry clone was recombined into the *Agrobacterium* destination

vector pPZP2017. *Agrobacterium* suspensions ($OD_{600} = 0.4$) were infiltrated into *Nb* and arugula leaves of 3-4-week-old plants using a 1-ml needleless syringe. Plants were returned to the growth chamber and imaged after 3 and 10 days-post-infiltration, and used in ddPCR experiments 14-days post-infiltration.

Droplet Digital PCR (ddPCR) experiments. Genomic DNA (gDNA) was extracted from leaves, 14 days after the treatment with pDNA-PEI-SWCNTs and *Agrobacterium*, via CTAB extraction modified from a previous method⁸. Briefly, 200 mg leaf tissue was ground in liquid nitrogen with a mortar and pestle, and the leaf powder was transferred into 600 μ l CTAB buffer (10 g CTAB, 50 mL 1 M Tris-HCl pH 8, 20 mL 0.5M EDTA pH 8, 140 mL 5 M NaCl and 5 g PVP). The mixture was vortexed well and incubated at 65°C for 45 minutes. 600 μ l chloroform:isopropanol (39:1) was added to mixture and vortexed well. The mixture was centrifuged at 18,000g for 10 minutes and the upper phase was transferred into a new microcentrifuge tube. 600 μ l isopropanol was added to the new tube, incubated 5 minutes at room temperature, and then mixed softly. The mixture was centrifuged at 18,000g for 10 minutes. The supernatant (isopropanol) was removed and 100 μ l 70% ethanol was added. The mixture was centrifuged at 18,000g for 10 minutes. The supernatant (ethanol) was removed as much as possible and the tube was left to dry at 37°C for 30 minutes. The gDNA pellet was resuspended in 200 μ l autoclaved MilliQ water and the concentration and purity was measured by Nanodrop. All gDNA samples were digested overnight with HindIII-HF in CutSmart buffer. 2 μ g gDNA was digested with 20U enzyme in a 50 μ l reaction volume for 16 hours at 37°C. Note that the restriction enzyme was selected so as not cut inside the reference or target gene. We have confirmed that the extracted genomic DNA does not contain any of the infiltrated plasmid DNA via several measures. First, 14-days incubation is assumed to be long enough for plasmid DNA to degrade inside the cells. Second, plasmid DNA is not present in any of the agarose gels we have run (ddPCR control gels in Supplementary Fig. 9). Last, all samples were treated

the same and if there was any plasmid DNA left at the time of PCR, it would be present not only in the *Agrobacterium* sample, but in all samples (which is not the case, as controls and DNA-PEI-SWCNT samples did not show any amplification with PCR).

ddPCR was performed via probe chemistry in a duplex assay for reference EF1 and target GFP genes. The GFP probe (5'-TGCCGTCCTCCTTGAAGTCG-3') was labeled with HEX at 5', Iowa Black Hole Quencher at the 3' end and with an internal ZEN quencher 9 nucleotides away from the 5' end. The EF1 probe (5'-AGGTCTACCAACCTTGACTGGT-3') was labeled with FAM at the 5' end, with Iowa Black Hole Quencher at the 3' end, and with internal ZEN quencher 9 nucleotides away from the 5' end. Primers used for GFP gene: 5'-GACTTCTTCAAGTCCGCCAT-3' and 5'-CGTTGTGGCTGTTGTAGTTG-3', primers used for EF1 gene: 5'-TCCAAGGCTAGGTATGATGA-3' and 5'-GGGCTCATTAATCTGGTCAA-3'. 20X probe-primer mixes (18 μ M PCR primers (each), 5 μ M probe) were prepared for both genes.

ddPCR reaction mixes were prepared according to the instructions in ddPCR Supermix for Probes (No dUTP) #1863024 kit. For each sample, we prepared 10 wells, each containing 100 ng digested gDNA, so that a total of 1 μ g DNA was screened for transgene integration for each sample. Droplets were generated with a QX200 droplet generator right after the ddPCR reaction mixes were prepared. 20 μ L of each sample mastermix was transferred to the sample row and 70 μ L droplet generation oil was transferred to the oil row in the droplet generation cartridge. After the droplets were generated, 40 μ L of droplets were transferred to a new 96-well plate and the plate was sealed for 5 s at 180°C in plate sealer. The PCR was run in a deep-well thermal cycler with the following PCR program: enzyme activation 95°C 10 min, denaturation 94°C 30 sec (40X), annealing/extension 60°C 1 min (40X), stabilization 98°C 10 min, and hold 4°C. The fluorescence of the droplets was measured 4 hours after PCR (kept in

the dark and at 4°C) with a QX200 droplet reader, and the results were analyzed with the Bio-Rad Quantasoft Pro Software.

Quantification of GFP protein amount in leaves. Month-old Nb leaves were infiltrated with either pDNA-PEI-SWCNTs or Agrobacterium solutions. Three days post-infiltration, leaves were harvested, weighed, then frozen and ground in liquid nitrogen to obtain powder. The powder was placed in a liquid nitrogen-cooled tube to which 350 µL of lysis buffer containing 10 mM Tris/HCl (pH 7.5), 150 mM NaCl, 1 mM EDTA, 0.1% NP-40, 5% glycerol, and 1% Cocktail was added. The tube was immediately vortexed for 2-3 seconds before being placed on ice while other samples were similarly harvested. All tubes were incubated in a 50°C water bath for 3 minutes, then centrifuged at 16,000 g for 40 minutes. The supernatant containing proteins were then transferred to a fresh tube.

A GFP-Trap (ChromoTek GFP-Trap_A) was used to purify and concentrate GFP present in the supernatant. For each sample, 25 µL of GFP-Trap beads was pipetted into ice-cold dilution buffer composed of 10mM Tris/HCl (pH 7.5), 150 mM NaCl and 0.5 mM EDTA. The beads were centrifuged at 2,500 g for 2 min at 4°C and the supernatant was discarded. This was then repeated twice. The beads were added to the supernatant along with 300 µL dilution buffer, and the tube placed on a tube rotator for 1 hour at 4°C. Samples were centrifuged at 2,500 g for 2 min at 4°C with the supernatant discarded. Then, 500 µL ice-cold dilution buffer was added to each sample, which was again centrifuged at 2,500 g for 2 min at 4°C with the supernatant discarded three times. The bound GFP was eluted by constant mixing with 50 µL 0.2M glycine at pH 2.5 for 30 s followed by centrifugation. The supernatant was transferred to a fresh tube and 5 µL 1M Tris Base pH 10.4 added for neutralization. The protein elution step was executed twice to obtain two tubes of approximately 55 µL each per sample.

A Qubit Protein Assay Kit (Invitrogen) was used to quantify the mass of GFP eluted. Briefly, 20 μ L of eluted protein was added to 180 μ L Qubit Working Solution. The samples were vortexed for 3 seconds and incubated at room temperature for 15 minutes. Standard calibrations and measurements were collected via a Qubit 4 Fluorometer.

Biolistic delivery of plasmid DNA. Nb and arugula seeds were sterilized in solution (20% bleach) for 30 minutes under gentle agitation, then washed three times with sterile water, plated on $\frac{1}{2}$ strength Murashige and Skoog (MS) medium, stratified for 2 days at 4°C before transferring to a 26°C incubator with 16-hour light: 8-hour dark cycle for growth. 3-wk-old leaves were placed onto semi-solid pre-shooting media [4.43 g/L of MS basal medium and vitamins; 36.43 g/L of mannitol; 36.43 g/L of sorbitol; 0.30g of casein enzymatic hydrolysate; 0.5 g/L of L-proline 2 mL/L of 2,4-D (1 mg/ml); pH 5.8; 3.5 g/L of Phytigel] in a 1.5-inch diameter circle in the center of the plate to facilitate bombardment and incubated at 25°C for 4 hours in the dark. 35S-GFP DNA plasmid (35sC4PPDKsGFPTYG) was coated onto 0.6 μ m gold nanoparticles (Bio-Rad): 1 mg of gold particles were mixed with 30 μ l of DNA construct (0.17 μ g/ μ l), 25 μ l of 5.0 M CaCl₂ and 20 μ l of 0.1 M spermidine and incubated on ice for 10 min. DNA-coated gold particles were collected at 14,000 rpm for 1 min, and the pellet was rinsed with 1 mL of absolute alcohol, resuspended in 85 μ l ethanol, and then immediately loaded onto the center of a macrocarrier (5 μ l each) and allowed to air dry. Biolistic bombardment was performed using a PDS1000/He particle bombardment system (Bio-Rad) with a target distance of 6.0 cm and a rupture pressure of 900 PSI. After bombardment, leaves were transferred to MS solid medium and imaged at 3 and 10 days-post-bombardment.

Comparison of CNT-mediated delivery with the gene-gun method

Biolistic (gene gun-based) DNA delivery is a preferred technique for transformation of plant species that are incompatible with *Agrobacterium*-based transformation. We next compared

CNT-mediated DNA delivery with biolistic particle DNA delivery by transforming mature arugula true leaves and cotyledons with the same GFP-encoding plasmid using a gene gun. Interestingly, with biolistic transformation, we obtained little GFP expression in arugula true leaves, and also observed sparse GFP expression only in some of the guard cells on the topmost surface of arugula cotyledons through high-pressure condition biolistic delivery (Supplementary Fig. 10). Since GFP expression is limited to the topmost layer of the cotyledons, it is likely that biolistic delivery cannot penetrate deep enough in the arugula leaf to enable transformation of sub-cuticle cell types, such as mesophyll cells, even though a wide range of gene gun pressures (up to 900 PSI) were also tested. To our knowledge, biolistic transformation of arugula leaves remains to be shown in the literature. Consequently, we tested the transformation of mature *Nb* plant leaves with biolistic transformation and successfully obtained GFP expression in mesophyll cells, most likely due to the fact that, as a model laboratory plant, *Nb* has a thinner and easy-to-penetrate leaf structure (Supplementary Fig. 10). These results demonstrate that depending on the plant species and tissue type, biolistic transformation can result in variable tissue penetration depth and lower expression efficiency compared to the CNT-mediated delivery.

Diffusion-reaction model to describe the spatial distribution of CNTs inside a leaf

After infiltration into the plant leaves, DNA-CNTs diffuse in the extracellular matrix while internalizing into plant cells. Consequently, there is a point where no nanocarrier is left in the extracellular matrix due to the consumption by cells proximal to the DNA-CNT infiltration area. We analyzed and modeled the spatial distribution of nanocarriers inside the leaf with a diffusion-reaction equation in which we implement a first order elementary reaction with a constant rate constant for metabolic consumption of nanocarriers. The model predicts an exponential decay in the concentration of nanocarriers with respect to distance from the infiltration area. To fit this mathematical model to our experimental results, we analyzed the

lateral profile of leaf GFP fluorescence expression obtained through confocal imaging as a proxy for nanocarrier diffusivity, and obtain good agreement between our diffusion-reaction model and GFP fluorescence localization ($R^2 = 0.996$, **Supplementary Fig. 8**).

The most general diffusion-reaction equation to describe the spatial distribution of CNT nanoparticles inside a leaf is:

$$\frac{\partial C}{\partial t} = D \left[\frac{\partial^2 C}{\partial x^2} + \frac{\partial^2 C}{\partial y^2} + \frac{\partial^2 C}{\partial z^2} \right] + F(C) \quad (1)$$

where C is the concentration of CNT nanocarriers carrying DNA or RNA, t is time, x , y , z denotes the distance from the infiltration area, D is the diffusion coefficient, and $F(C)$ is a function for nanocarrier consumption in the leaf.

We have assumed the following to simplify the general equation:

1. 1D in Cartesian coordinates
2. Steady-state; $\left. \frac{\partial C}{\partial t} \right|_{ss} = 0$
3. First order elementary reaction with constant rate constant; $F(C) = -kC$

With these assumptions, Equation (1) simplifies to:

$$D \frac{\partial^2 C}{\partial x^2} = kC \quad (2)$$

where k is the metabolic consumption rate of our nanocarrier by plant leaf cells.

The boundary conditions are:

$$C(x=0) = C_o \quad \text{Known infiltration concentration at the infiltration point}$$

$$\left. \frac{\partial C}{\partial x} \right|_L = 0 \quad \text{No flux outside the impermeable leaf boundary}$$

The constants k and D are calculated as follows:

$$k^1 = 0.52 \text{ min}^{-1}$$

$$D^2 = 0.75 \text{ nm}^2/\text{ns}$$

Then, α is defined as square root of the k to D ratio:

$$\alpha = \sqrt{\frac{k}{D}} = 3 \times 10^{-6} \text{ nm}^{-1}$$

With these given boundary conditions, solution to Equation (2) is:

$$C(x) = C_0(\cosh \alpha x - \tanh \alpha L \sinh \alpha x) \quad (3)$$

Inserting the constants k and D into the solution, we get:

$$C(x) = C_0(\cosh \alpha x - \sinh \alpha x) \quad (4)$$

which can be further simplified by using the definition of hyperbolic functions:

$$C(x) = C_0 e^{-\alpha x} \quad (5)$$

The solution for the simplified diffusion-reaction equation is thus an exponential decay function, which suggests that the concentration of our nanocarriers decreases exponentially from the DNA-CNT infiltration area. To fit this mathematical model to our experimental results, we used GFP fluorescence measurements obtained through confocal imaging as a proxy for nanocarrier concentration and internalization into plant cells (**Supplementary Fig. 8**).

Our fitting results demonstrate good agreement between our model and fluorescence imaging experiments for the exponential decay function solution. The goodness estimates of the fits are 0.9953 and 0.996 for CNTs loaded with linear DNA (lDNA) and plasmid DNA (pDNA), respectively. However, experimental GFP fluorescence data inside the leaves exhibit a stationary phase prior to the exponential decay phase, which we predict occurs due to the fact that closer to the infiltration area, there is a surplus of DNA-CNT conjugates relative to available plant leaf cells. As such, the local concentration of CNTs is higher than can be captured by GFP expression, such that CNT internalization by cells proximal to the infiltration area underestimates the effective concentration of CNT nanocarriers.

The effect of CNT surface chemistry on delivery efficiency

Our results suggest that the CNT surface chemistry is an important factor for biomolecule delivery into plant cells. The observed results can be explained by different DNA binding affinities to CNT surfaces in the two DNA grafting methods. The predominant DNA-CNT binding interaction in the case of dialysis is π - π stacking. In contrast, electrostatic attraction between PEI-CNTs and DNA is the predominant binding interaction for the electrostatic grafting method. We propose that the smaller equilibrium dissociation constant³ and higher binding energy value^{4,5} for electrostatic attraction compared to π - π stacking interactions increase the stability of the DNA-CNT complex as it traverses the cell wall, plasma membrane, and nuclear envelope, thus increasing the delivery efficiency of DNA to the plant cell. Worthy of note, for electrostatically-loaded DNA, we also observe statistically significantly higher protein expression efficiencies with CNT conjugates loaded with plasmid (pDNA) compared to linear (lDNA) conjugates. We hypothesize that this difference in transformation efficiency is due to the decreased cytosolic degradation rate of pDNA compared to lDNA in eukaryotic cells, as lDNA is prone to degradation by both endo- and exonucleases⁶, while pDNA is only degraded by endonucleases (as it does not contain free ends).

Additional considerations of PEI-CNTs and their use as a plant transformation tool

After preparation, PEI-CNT complexes are stable for at least 2 months at 4°C and can be stored long-term at -20°C by freezing. We show that freeze-thaw cycles do not affect the colloidal stability of PEI-CNTs, and thawed PEI-CNTs remain active for DNA loading and transformation (**Supplementary Fig. 11**). The 2-month solution-phase stability of PEI-CNT complexes facilitates rapid loading of DNA onto CNTs through a 30-minute co-incubation of DNA vectors with PEI-CNTs. Our platform is also scalable and amenable to high throughput applications. The preparation of PEI-CNTs and DNA loading can be scaled by changing the

amounts of constituents while keeping their mass ratio constant (see Methods for details of the PEI-CNT reaction and DNA loading). Additionally, with CNTs, loading one plasmid versus tens of plasmids will take the same amount of time, as the only required step is mixing of plasmids with CNTs. Conversely, if such high-throughput applications are desired with *Agrobacterium* transformation, the researcher first needs to transform *Agro* bacterial strains separately with each plasmid, grow each strain, and activate the T-DNA (3-4 days) before introducing *Agrobacteria* into plants as a mixture of each strain solution.

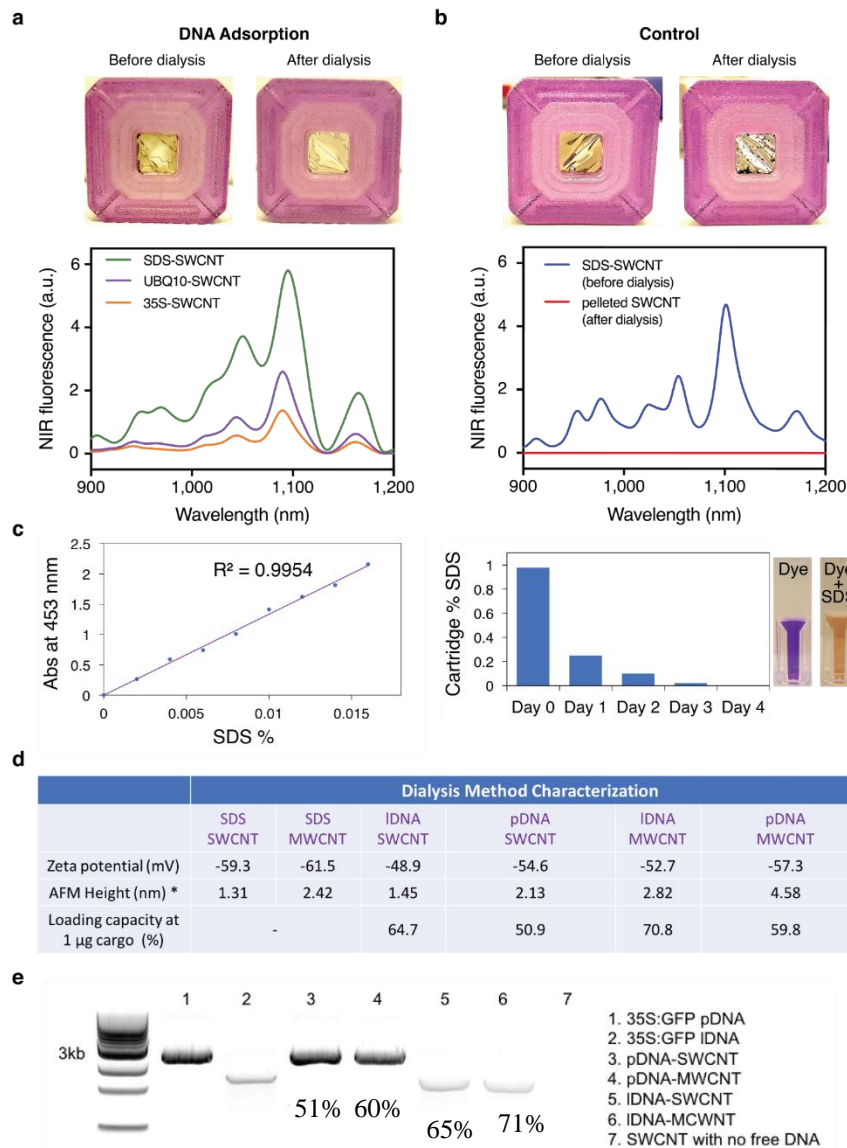
A simple calculation reveals that this study's CNTs and their necessary chemistries cost less than 3 dollars per infiltration, and do not require the relatively high cost associated with gene gun equipment and gold particles commonly used in biolistic delivery. Below, we detail the calculation to estimate the cost per infiltration:

CNT	\$0.22
PEI	\$0.01
DNA preparation	\$0.24
All consumables	\$0.29
Utilities	\$0.20
Labor	\$2.00
Total	\$2.96/infiltration

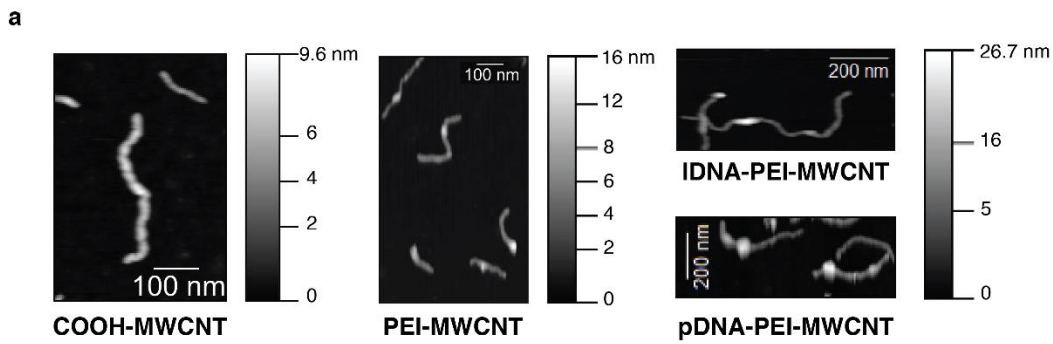
The EPA (regulation #40 CFR 721.10929) classifies CNTs under the "Toxic Substances Control Act" as distinct from carbon and graphite on the grounds that sufficient information is known about bulk-sized carbon and graphite, whereas insufficient information is known about these same materials at the nano-scale. This regulation necessitates certain approvals for the synthesis and distribution of CNTs, and it is required to handle all dry CNT materials inside a

chemical fume hood with proper protective personal equipment until CNT materials are in solution phase, at which point they may be handled outside a chemical hood.

Specifically regarding genetic transformation of edible plants with CNTs, we note that the transformed plant material constitutes the experimental generation T₀. Plants genetically edited with CNTs would undergo several generations of progeny production before their seeds are brought to market, and thus edible plants would constitute generations that have never undergone exposure to CNTs.



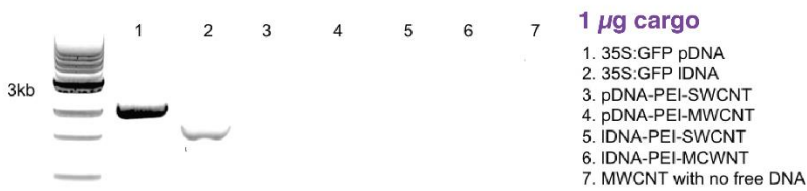
Supplementary Figure 1. Confirmation of DNA adsorption on CNTs through dialysis and loading efficiency characterization. **(a)** Adsorption of DNA on CNTs is confirmed through a 5-nm wavelength shift in the SWCNT nIR fluorescence emission spectra. No CNT precipitation is observed after dialysis with DNA, confirming that DNA adsorption follows SDS desorption from CNTs **(b)** Control dialysis aliquots of SDS coated CNTs in the absence of DNA show rapid CNT precipitation and lack nIR fluorescence, confirming DNA adsorption and SDS desorption in the sample 'a' dialysis. **(c)** Stains-all dye changes color from purple to yellow in the presence of SDS. A standard curve correlates absorbance of dye at 453 nm to %SDS concentration. The standard curve is used to detect %SDS left in the dialysis cartridge at Day 0, 1, 2, 3 and 4. At day 4, when dialysis is terminated, there is no SDS left in the cartridge. **(d)** Characterization of nanoconjugates prepared via dialysis; zeta potential, AFM height, and loading efficiency at 1 μg DNA is presented. **(e)** Due to their large size, DNA-CNT conjugates do not run into the agarose gel, hence the bands visualized in the gel are free DNA bands. By measuring the intensity of unloaded DNA bands normalized with respect to the intensities of lane 1 and 2, which are loaded with a known amount of pDNA and IDNA, the loading efficiency of IDNA onto SWCNTs is calculated to be 64.7%, pDNA onto SWCNTs is 50.9%, IDNA onto MWCNTs is 70.8%, and pDNA onto MWCNTs is 59.8% with the dialysis method.



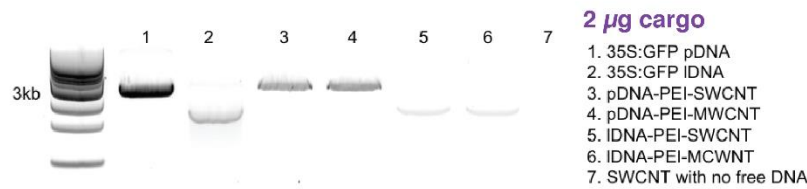
b

	Electrostatic Method Characterization							
	COOH SWCNT	COOH MWCNT	PEI SWCNT	PEI MWCNT	IDNA-PEI SWCNT	pDNA-PEI SWCNT	IDNA-PEI MWCNT	pDNA-PEI MWCNT
Zeta potential (mV)	-54.7	-41.7	+42.4	+46.3	+36.4	+30.7	+38.7	+33.4
AFM Height (nm)	1.37	6	8.3	12.1	14.75	16.43	22.8	26.7
AFM Length (nm)	820	1250	616	785	610	590	725	700
Loading capacity at 1 μ g cargo (%)			-		100	100	100	100
Loading capacity at 2 μ g cargo (%)			-		72.6	65.2	73.1	63.8

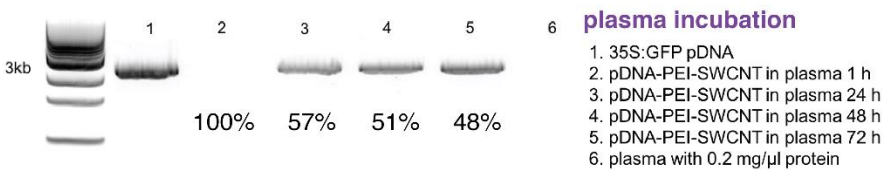
c



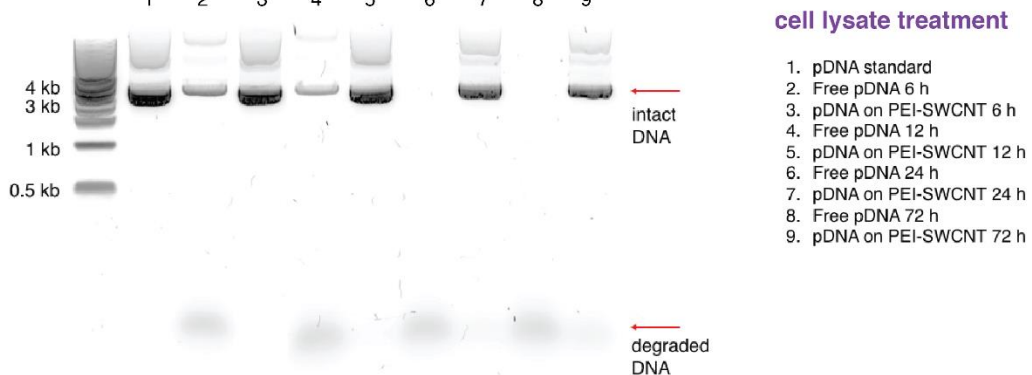
d



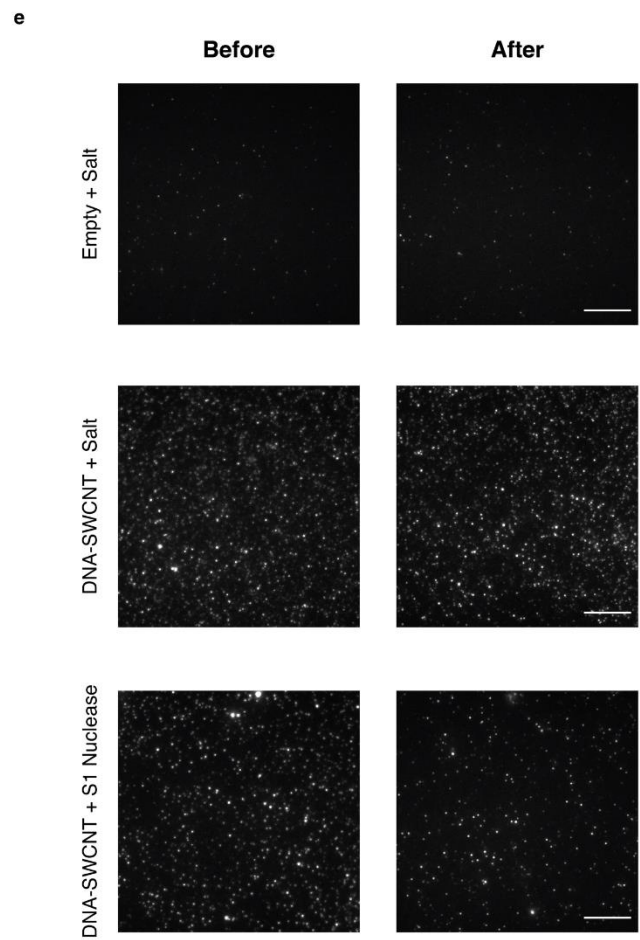
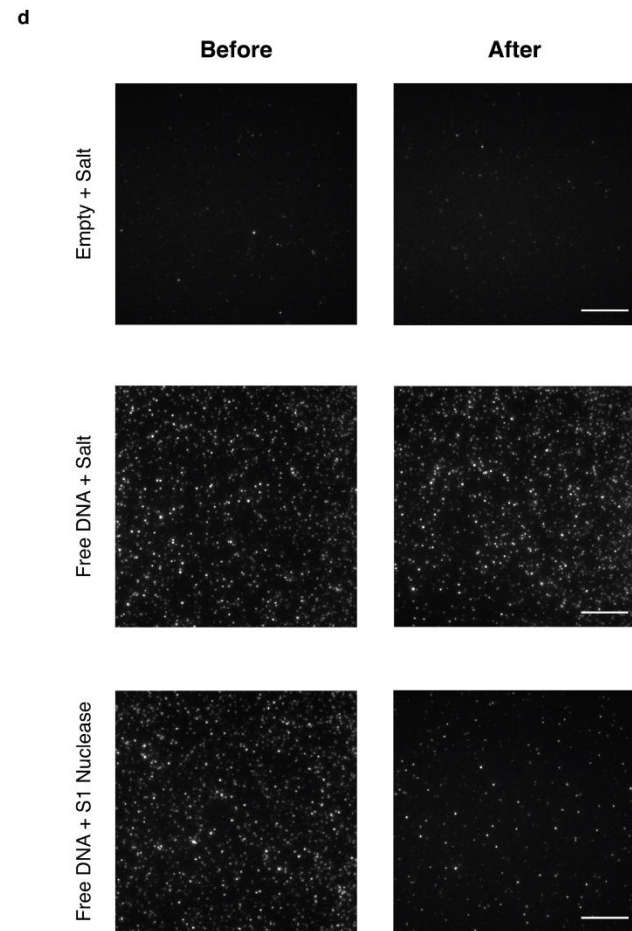
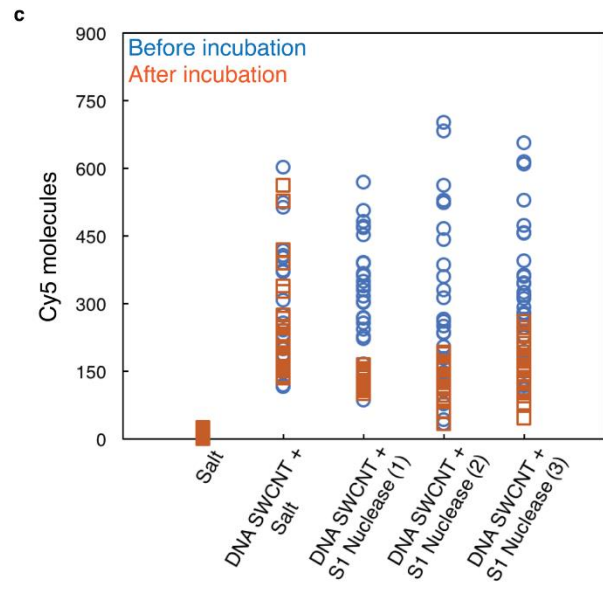
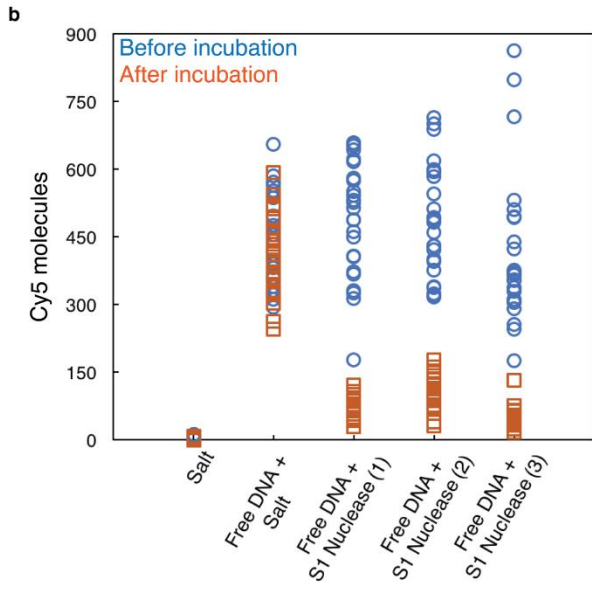
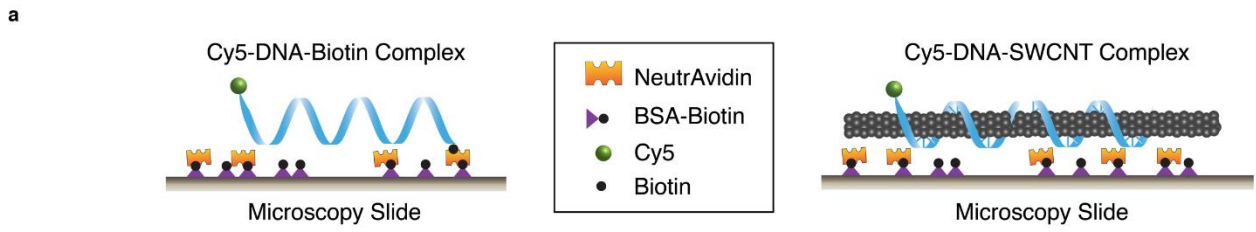
e



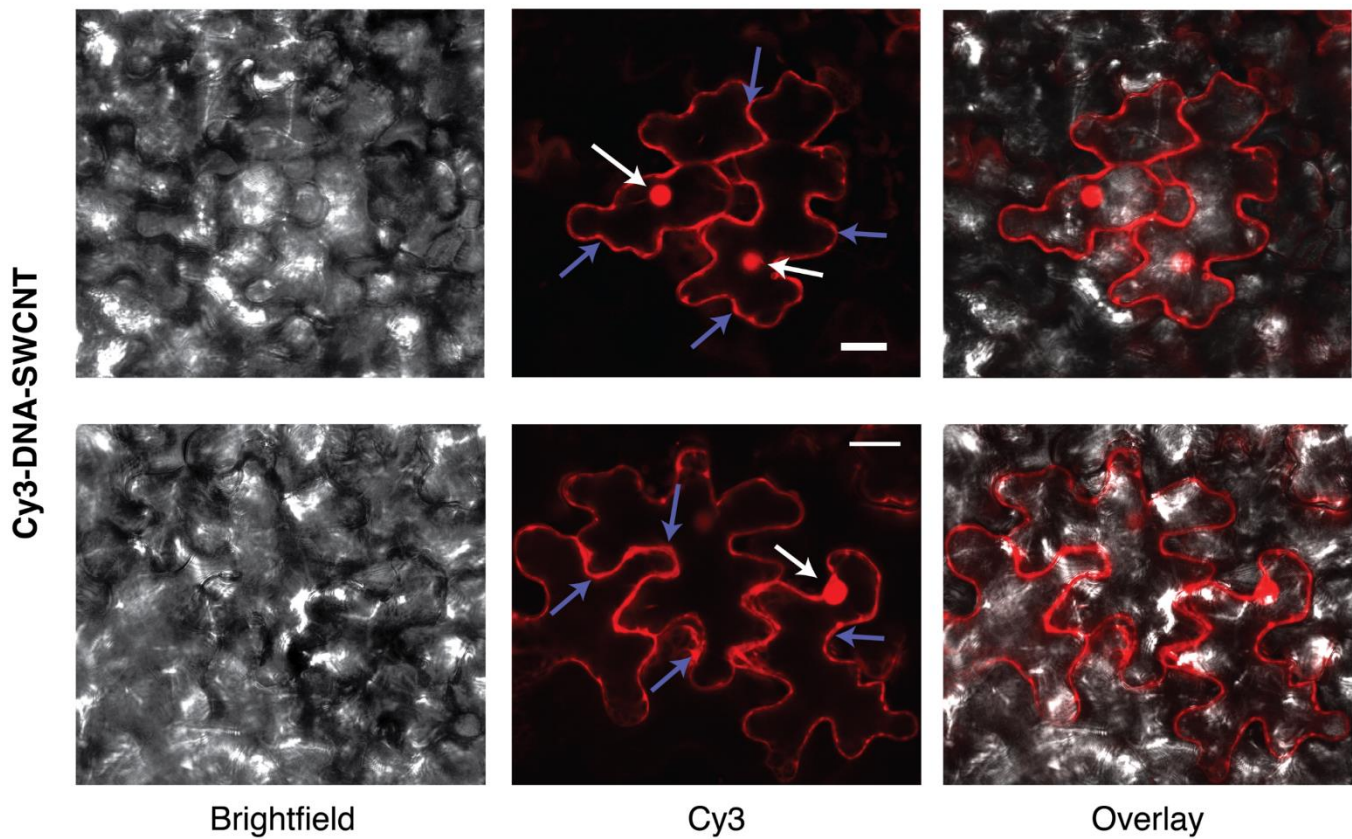
f



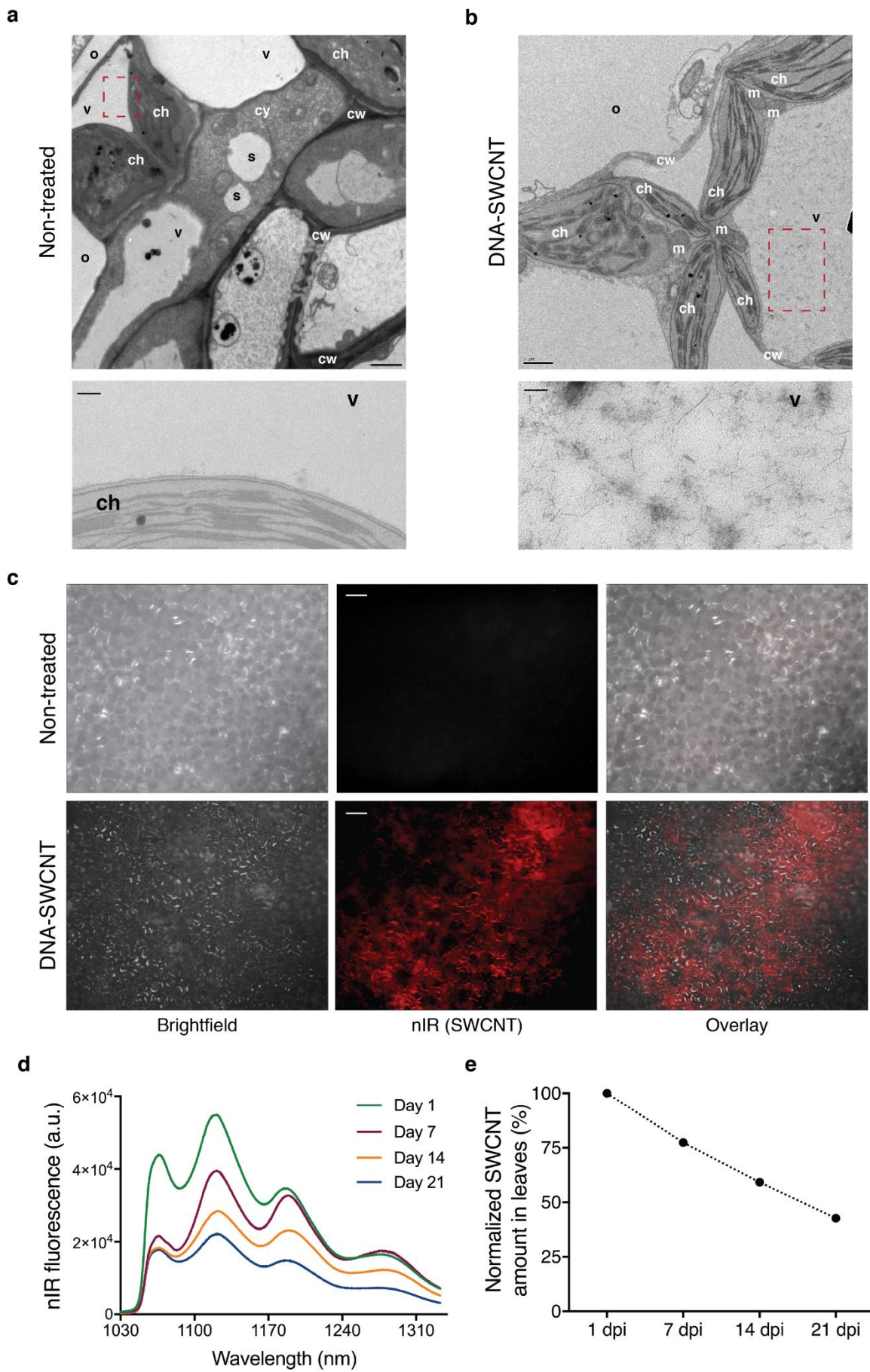
Supplementary Figure 2. Confirmation of synthesis and DNA adsorption on PEI-CNTs with loading efficiency characterization. **(a)** Representative AFM imaging of MWCNTs prepared through electrostatic grafting. AFM imaging of carboxylated MWCNT nanoparticles before and after reaction with PEI confirms covalent PEI attachment with MWCNT heights of 6 ± 0.60 and 12.1 ± 0.87 nm for COOH- and PEI-MWCNTs, respectively. AFM also reveals that MWCNT nanoparticle height increases from 12.1 ± 0.87 to 22.8 ± 2.19 nm after incubation with DNA vectors, further confirming DNA vector grafting onto MWCNTs. **(b)** Characterization of nanoconjugates prepared with the electrostatic method of DNA loading on CNTs: zeta potential, AFM height and length, and loading capacity of 1 and 2 μg DNA is presented. **(c)** As there is no unbound DNA running into the agarose gel when 1 μg PEI-CNTs are loaded with 1 μg DNA, all loading capacities regardless of DNA conformation or nanotube type are 100% when a 1:1 DNA:CNT mass ratio is used. **(d)** When 2 μg PEI-CNTs are loaded instead with 1 μg DNA, we calculate a 72.6% loading efficiency of IDNA onto SWCNTs, a 65.2% loading efficiency of pDNA onto SWCNTs, a 73.1% loading efficiency of IDNA onto MWCNTs, and a 63.8% loading efficiency of pDNA onto MWCNTs (band intensities are normalized with respect to the intensities of lane 1 and 2, which are loaded with a known amount of pDNA and IDNA). **(e)** pDNA-PEI-CNTs are incubated in plasma containing 0.2 mg/ μL total protein to approximate the DNA desorption rate in intracellular conditions. Results show that even after a 72-hour incubation in plasma at 21°C, almost half of the DNA is still adsorbed on PEI-CNTs. **(f)** Agarose gel electrophoresis of free pDNA and pDNA on PEI-CNTs incubated with plant lysate solution for 6, 12, 24, and 72 hours to determine pDNA protection against nuclease degradation on PEI-CNTs. All DNA pieces (degraded and intact) are desorbed from the CNT surface after cell lysate treatment and prior to running the gel.



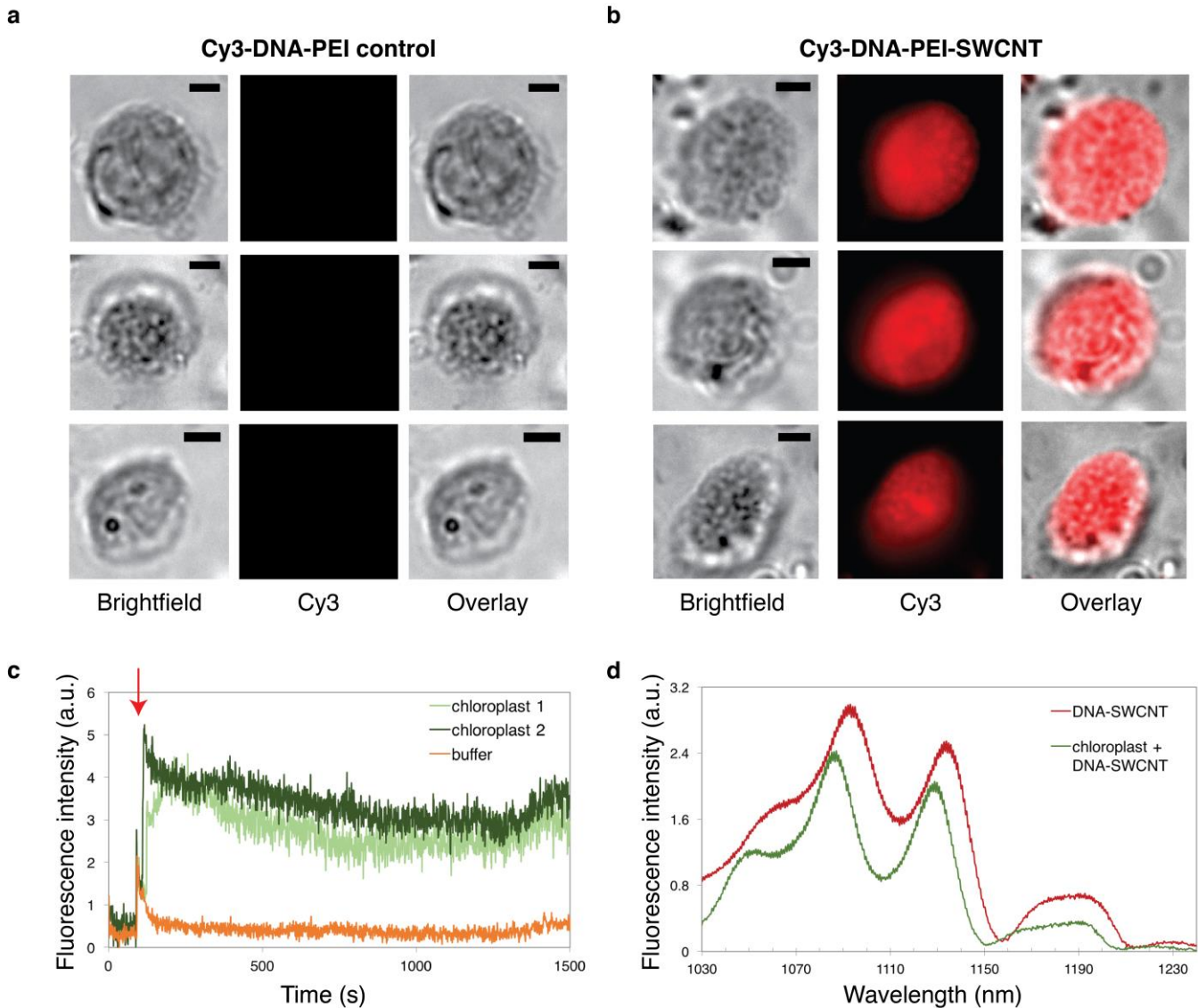
Supplementary Figure 3. Single molecule TIRF (smTIRF) microscopy demonstrates DNA protection against nuclease degradation when on CNTs **(a)** Schematics of microscopy slides for immobilization of Cy5-DNA-Biotin and Cy5-DNA-CNT complexes. The microscopy slide surface is first coated with BSA-Biotin, then incubated with NeutrAvidin. Cy5-DNA-Biotin is immobilized on the surface via Biotin-NeutrAvidin attraction, and Cy5-DNA-CNT is next immobilized on the surface via non-specific interaction of NeutrAvidin with CNTs **(b)** Raw smTIRF data for empty channel rinsed with salt solution, free DNA incubated with salt solution, and three experimental replicates of free DNA incubated with 2.8U/ μ L S1 nuclease, blue: before incubation and orange: after incubation. Data from 30 fields of view plotted for each sample before and after nuclease treatment. **(c)** Raw smTIRF data for empty channel rinsed with salt solution, DNA-CNT incubated with salt solution, and three experimental replicates of DNA-CNT incubated with 2.8U/ μ L S1 nuclease, blue: before incubation and orange: after incubation. Data from 30 fields of view plotted for each sample before and after nuclease treatment. All channels contain BSA-Biotin and NeutrAvidin. **(d)** Representative smTIRF microscopy images for each sample of free DNA before and after incubation with salt and 2.8U/ μ L S1 nuclease. Scale bars, 10 μ m. **(e)** Representative TIRF microscopy images for each sample of DNA-CNTs before and after incubation with salt and 2.8U/ μ L S1 nuclease. Scale bars, 10 μ m.



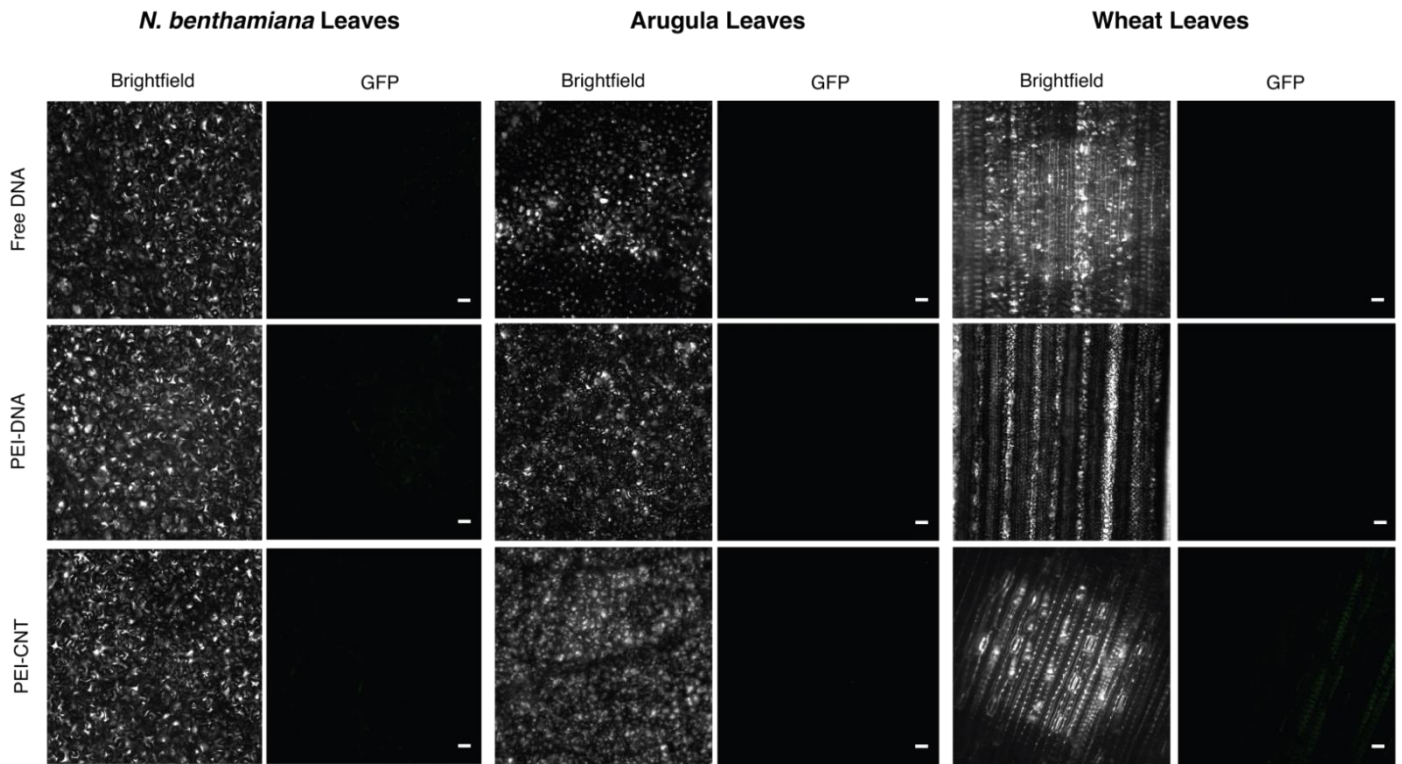
Supplementary Figure 4. Cy3-DNA-CNT subcellular localization in wild type *Nicotiana benthamiana* intact leaves, still attached to plants, with high-resolution confocal microscopy. Cy3 fluorescence is observed both in the cell cytosol and nuclei 6 hours after infiltration of Cy3-DNA-CNT conjugates. White arrows show cell nuclei and blue arrows show cell cytoplasm containing Cy3-DNA-CNT conjugates. Scale bars, 25 μ m. All experiments are done with intact leaves attached to healthy plants.



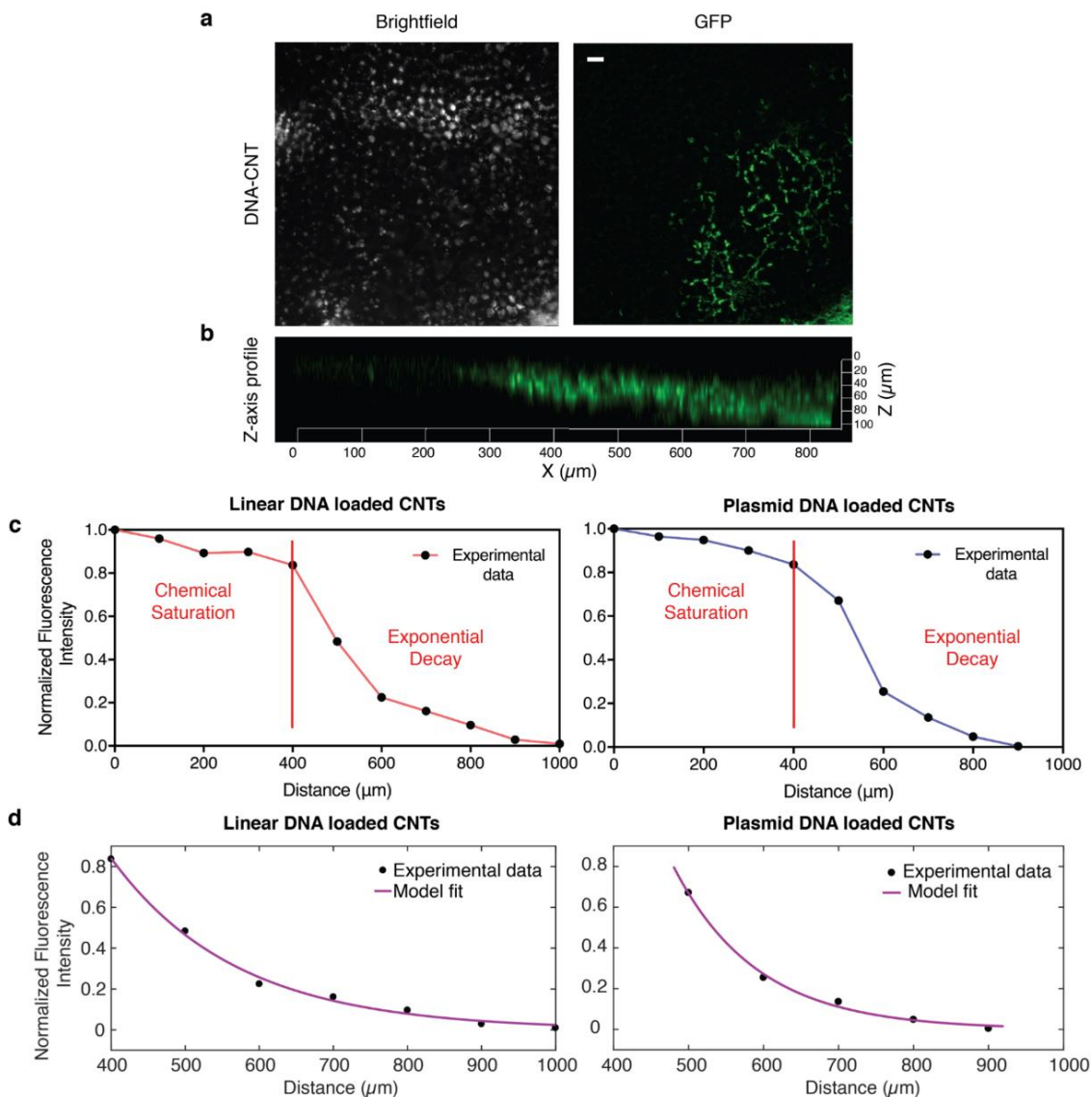
Supplementary Figure 5. CNT internalization and long-term fate inside plant leaf tissues. Annotated TEM images of non-treated (**a**) and DNA-CNT treated leaves (**b**). Nanoparticles are only observed inside the cells of DNA-CNT treated leaves. Scale bar for the full-size image in (**a**) is 2 μm , and for the zoomed-in image 200 nm. Scale bar for the full-size image in (**b**) is 1 μm and for the zoomed-in image 100 nm. TEM annotations are o: outside the cell, v: vacuole, ch: chloroplast, cy: cytoplasm, cw: cell wall, s: starch and m: mitochondria. (**c**) Near-infrared fluorescence microscopy of DNA-CNTs in mature *Nb* leaves. Plant cell internalization and diffusion of DNA-CNTs is demonstrated via near-infrared fluorescence imaging. CNTs are excited with a 350 mW 721 nm laser. Non-treated leaf does not show SWCNT-related near-infrared fluorescence, as expected, whereas the leaf infiltrated with DNA-loaded CNTs demonstrates strong near-infrared fluorescence. Scale bars, 50 μm . (**d**) nIR fluorescence spectra of DNA-CNTs inside infiltrated leaves per area 1, 7, 14, and 21-days past infiltration (dpi). (**e**) Area under the curve from (d) showing that the amount of CNTs inside the leaf per area decreases gradually from Day 1 to Day 21. All experiments are done with intact leaves attached to healthy plants.



Supplementary Figure 6. Cy3-DNA-PEI-CNT and DNA-CNT localization in chloroplasts extracted from wild type *Nicotiana benthamiana* leaves. **(a)** No Cy3 fluorescence is observed in extracted chloroplasts when chloroplasts are incubated with Cy3-DNA-PEI without CNTs. **(b)** Strong Cy3 fluorescence is observed in representative extracted chloroplasts when chloroplasts are incubated with Cy3-DNA-PEI-CNTs. Scale bars, 1 μm . **(c)** Extracted chloroplasts are also incubated with a non-fluorophore labeled single-stranded DNA-CNT suspension and imaged with the intrinsic nIR fluorescence of CNTs with nIR microscopy to assess CNT uptake into chloroplasts. nIR fluorescence intensity of two representative chloroplasts shows an increase in nIR fluorescence upon addition of DNA-CNT, whereas chloroplast-free background does not show a sustained change in nIR fluorescence. **(d)** nIR fluorescence spectra of DNA-CNTs before and after internalization into extracted chloroplasts shows a ~ 6 nm wavelength shift due to lipid adsorption on CNTs while traversing the chloroplast lipid bilayer, as demonstrated previously⁷.

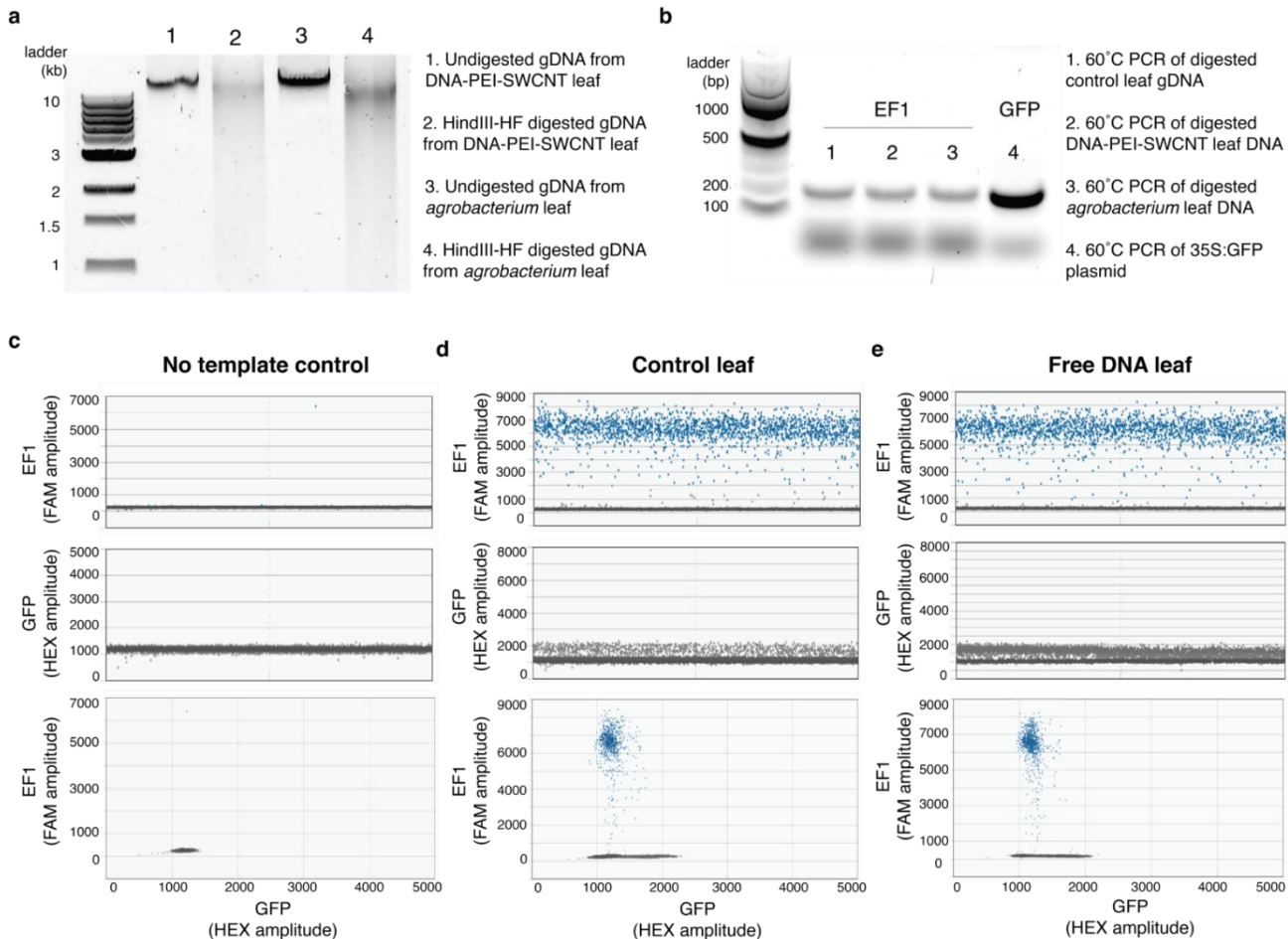


Supplementary Figure 7. Control studies for DNA-CNT delivery and GFP protein expression in mature *Nicotiana benthamiana*, arugula, and wheat leaves. When free plasmid DNA, or PEI-DNA, or PEI-CNT is delivered, no GFP expression is detected in any plant species via confocal microscopy at 72h post-infiltration, as shown by representative confocal images obtained with the same optical parameters with DNA-CNT induced GFP expression imaging. Scale bars, 50 μ m. All experiments are done with intact leaves attached to healthy plants.

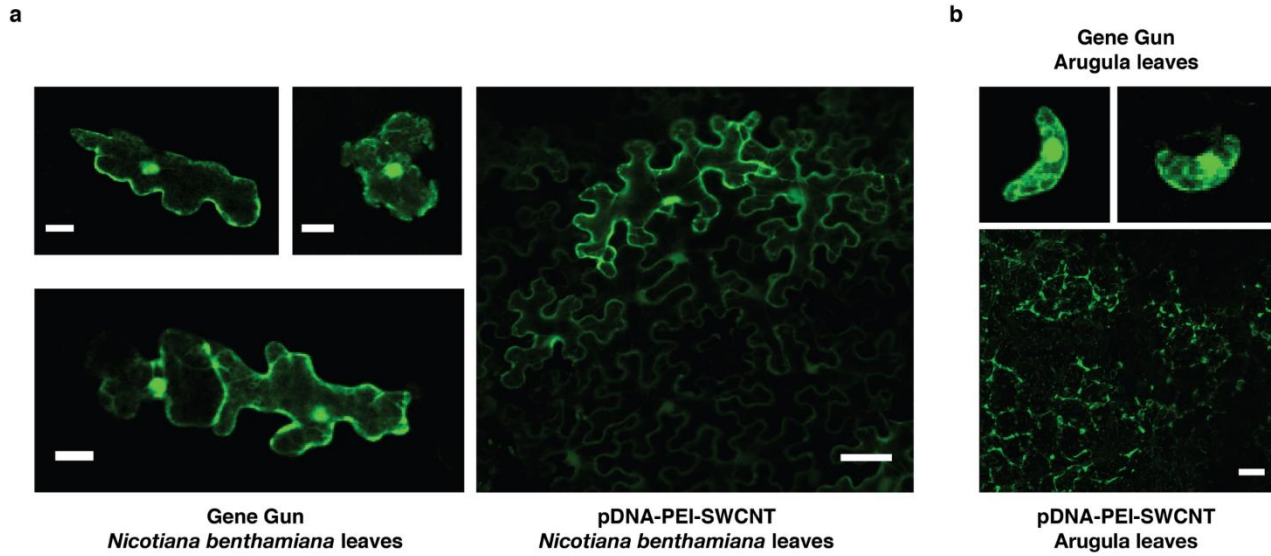


Supplementary Figure 8. Spatial distribution analysis of CNT nanocarriers inside the plant leaf modeled by a diffusion-reaction equation. **(a)** Confocal image of a DNA-CNT infiltrated arugula leaf shows the spatial distribution of GFP expression at a field of view farther away from the infiltration area (roughly bottom right corner), showing GFP expression begins to disappear when further from DNA-CNT exposure. Scale bar, 50 μm . **(b)** Z-axis profile of the same leaf area demonstrating the z-axis distribution of GFP from the leaf abaxial to adaxial surfaces. **(c)** Experimental data obtained from confocal imaging of GFP shows two phases for DNA-CNT diffusion: a stationary chemical saturation phase and an exponential decay phase of GFP fluorescence (Experimental data points are connected for clarity). **(d)** Spatial distribution of nanocarriers inside the plant leaf is modeled and plotted with a first order diffusion-reaction equation. The model predicts an exponential decay in the concentration of nanocarriers with respect to the distance from the infiltration area. To fit the mathematical model (purple trace) to our experimental results (black dots), we analyzed the lateral profile of plant leaf GFP fluorescence intensity measurements obtained through confocal imaging as a proxy for nanocarrier diffusivity, and obtained good agreement between our diffusion-reaction model and GFP expression in the leaf tissue ($R^2 = 0.9953$ for plasmid DNA loaded CNTs and $R^2 = 0.996$ for linear DNA loaded CNTs). All experiments are done with intact leaves attached to healthy plants.

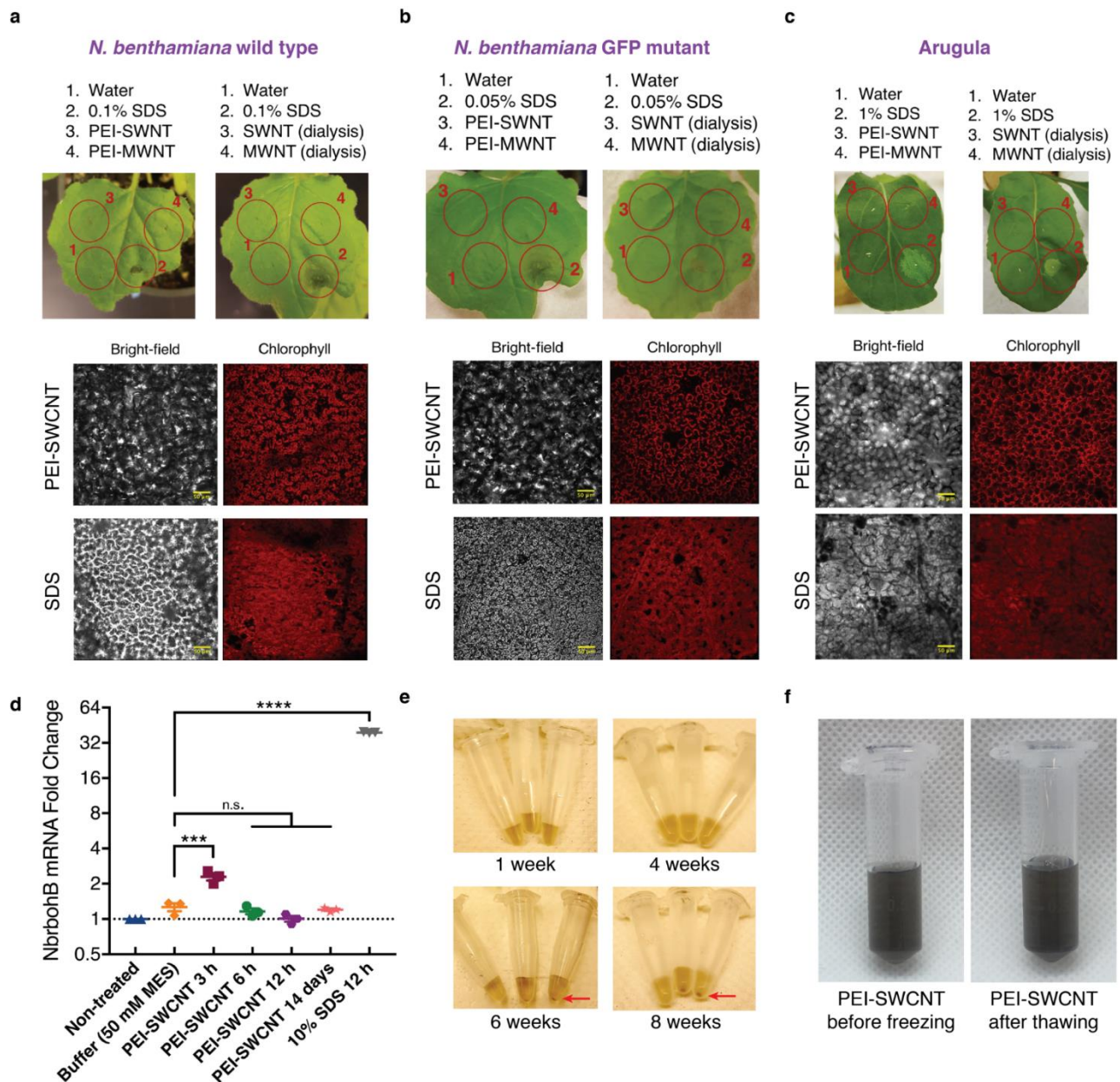
Droplet digital PCR (ddPCR) is a relatively new method that enables high-precision and absolute quantification of nucleic acid target sequences by partitioning each sample into 20,000 droplets, which then through PCR amplification within each droplet, count fluorescent positive and negative droplets specific to the DNA sequence of interest. In our case, we screen for GFP transgene integration into the plant host genome, and use elongation factor 1 (EF1) as a reference gene and thus positive control.



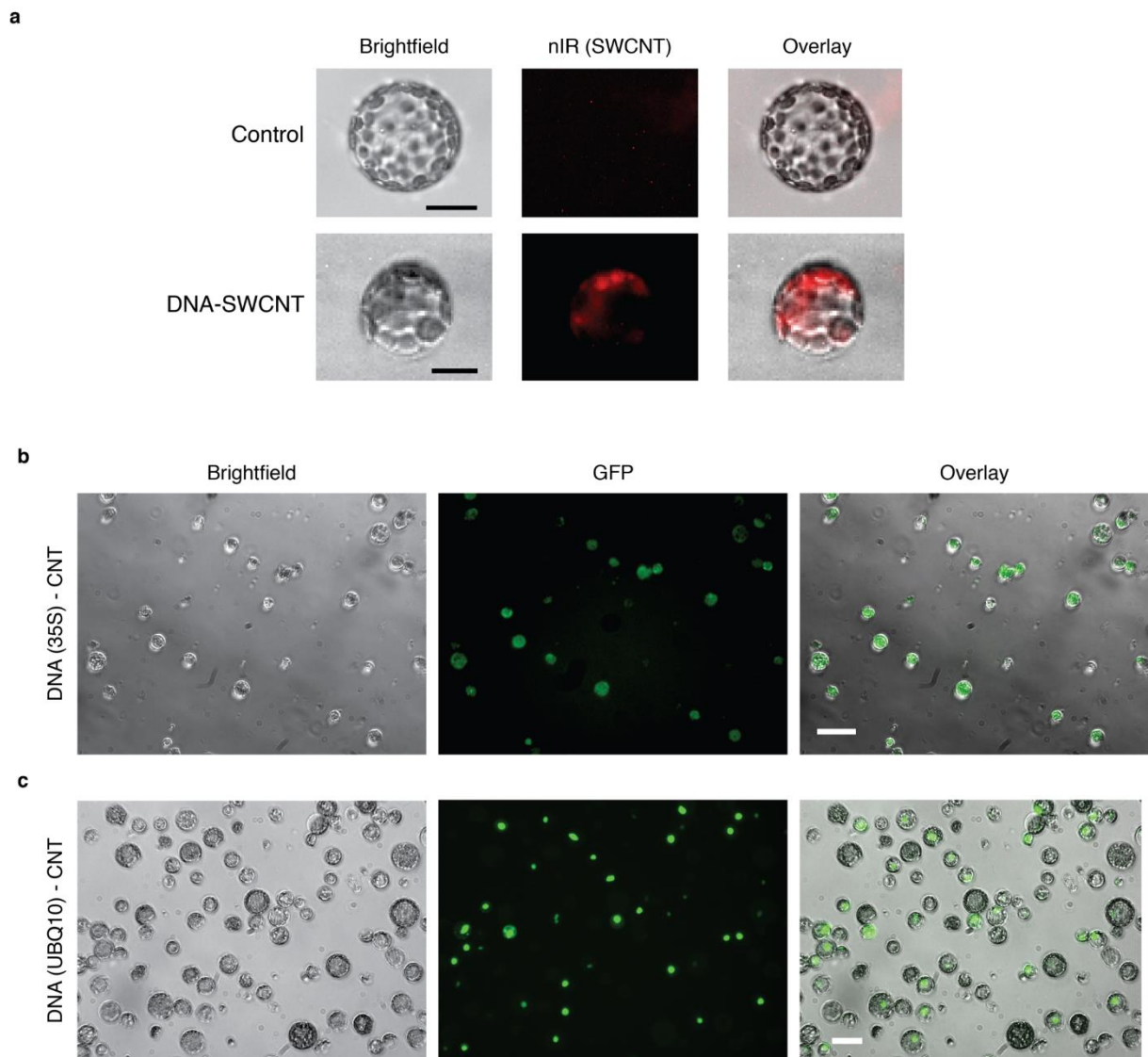
Supplementary Figure 9. Droplet digital PCR (ddPCR) control experiments (a) Genomic DNA extraction and digestion with HindIII-HF restriction enzyme is optimized for ddPCR experiments. Agarose gel electrophoresis showing successful and pure genomic DNA extraction in wells 1 and 3. Wells 2 and 4 show successful genomic DNA digestion of DNA-PEI-CNT and agroinfiltrated leaves. No plasmid DNA contamination was observed in any of our genomic DNA extractions. (b) Agarose gel electrophoresis shows that EF1 and GFP primers perform optimally during PCR at 60°C with the correct amplicon at size ~200 bp both for the EF1 reference gene and also for the GFP target gene. (c) ddPCR run showing no amplification of the EF1 or GFP genes in the no template control well. (d) ddPCR run result showing significant amplification of the EF1 gene but no amplification of the GFP gene in the control (non-treated) leaf. (e) ddPCR run result showing significant amplification of the EF1 gene but no amplification of the GFP gene in the free plasmid DNA infiltrated leaf, as expected. The EF1 gene is labeled with a FAM tagged probe and the GFP gene is labeled with a HEX tagged probe. Both probes are initially quenched with a 3' Iowa Black Hole Quencher and a ZEN internal quencher manufactured by IDT. All experiments are done with intact leaves attached to healthy plants.



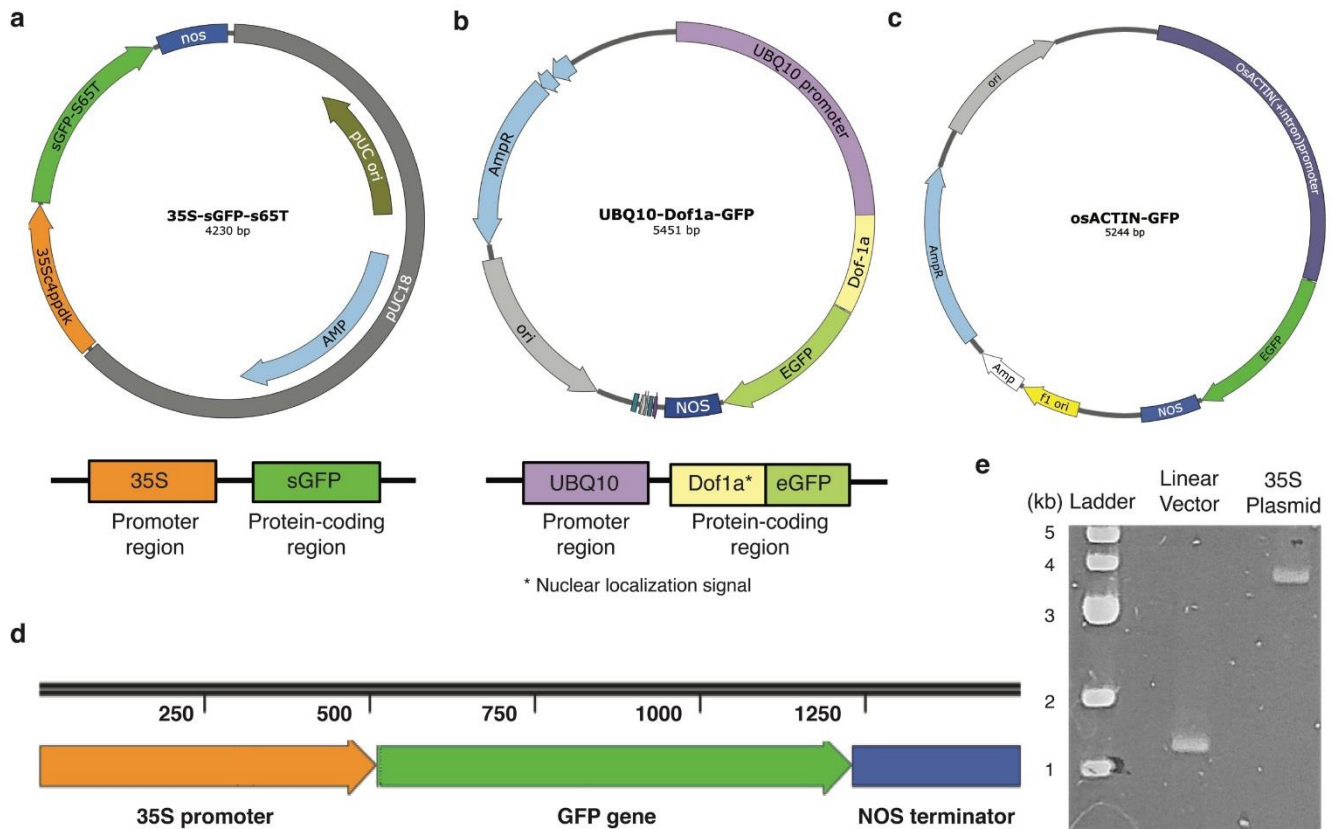
Supplementary Figure 10. Comparison of CNT-mediated transformation with biolistic (gene gun) based transformation. **(a)** In *Nicotiana benthamiana* leaves, gene gun-mediated sparse GFP expression is observed in the leaf mesophyll cells, whereas expression was more dispersed when delivered via pDNA-PEI-CNTs. **(b)** Gene gun-mediated GFP expression is only observed sparsely in the guard cells of arugula cotyledons, and no to little expression is observed in the true arugula leaves (not shown). With pDNA-PEI-CNTs, GFP expression was also more dispersed in true arugula leaves. All scale bars, 20 μ m. Gene gun experiments are performed with detached leaves.



Supplementary Figure 11. Tissue damage, short and long-term toxicity of PEI-CNTs in leaves and long-term PEI-CNT stability. **(a)** Tissue damage induced by infiltration of water, SDS, PEI-SWCNT and PEI-MWCNT (electrostatic), and SWCNT and MWCNT (dialysis) samples are tested in mature *Nb* wild type leaves, **(b)** mature *Nicotiana benthamiana* GFP mutant leaves and **(c)** mature arugula leaves. None of the CNT formulations cause tissue damage compared to water control, and only the positive control SDS infiltrated leaves show significant tissue damage detected by visual observation and by confocal imaging. Scale bars, 50 μ m. **(d)** NbrbohB stress gene expression levels are measured with qPCR, whereby NbrbohB expression doubles at 3 h but returns to baseline 6 h following infiltration with PEI-CNTs. No long-term toxicity is observed for PEI-CNT infiltrated leaves. **(e)** Photos showing the 4°C stability of pDNA loaded PEI-SWCNTs for more than 4-weeks, and by week 6 some CNT pelleting begins to occur. Red arrows denote the pelleting of CNTs. **(f)** PEI-CNTs can be stored longer-term by freezing at -20°C, and upon thawing PEI-CNTs are stable and remain active for DNA loading and transformation (data not shown). All experiments are done with intact leaves attached to healthy plants.



Supplementary Figure 12. CNT internalization into protoplasts and transformation with plasmid DNA loaded CNTs prepared via dialysis. (a) Nanoparticle internalization into isolated *Nicotiana benthamiana* protoplast is verified by imaging the intrinsic nIR fluorescence of CNTs following 6 hours of incubation with protoplasts. Scale bars, 10 μm . (b) Isolated arugula protoplasts are incubated with 35S plasmid DNA loaded CNTs, in which the plasmid is lacking a nuclear localization signal. In this case, GFP expression is observed inside the cell everywhere. Scale bars, 25 μm . (c) Isolated arugula protoplasts are incubated with UBQ10 plasmid DNA loaded CNTs, which contains a nuclear localization signal. In this case, GFP expression is observed only in the nucleus. No observable adverse effects to protoplast viability are observed with either DNA-CNT formulation via dialysis. Scale bars, 25 μm . Protoplasts isolated from intact leaves attached to healthy plants.



Supplementary Figure 13. Plasmids used in the current study and confirmation of plasmid linearization through PCR. (a) Plasmid map for 35S dicot plasmid DNA encoding sGFP-S65T that lacks a nuclear localization signal for the expressed GFP protein. (b) Plasmid map for UBQ10 dicot plasmid DNA encoding eGFP that contains a nuclear localization signal (Dof1a) for the expressed GFP protein. (c) Plasmid map for osACTIN monocot plasmid DNA encoding eGFP that lacks a nuclear localization signal for the expressed GFP protein. (d) Sanger sequencing of the linear amplicon shows error-free amplification of the promoter, GFP gene, and NOS terminator regions of 35S dicot plasmid. (e) Linearization of the 35S plasmid is accomplished through PCR amplification, and the linear amplicon that is run on a 1% agarose gel via electrophoresis shows the expected linear DNA size of 1.5 kbp (35S plasmid DNA runs a bit “smaller” than its actual size of 4.2 kb due to its supercoiled conformation, but has been sequenced to verify its correct sequence).

References

1. Hicks, K. O., Fleming, Y., Siim, B. G., Koch, C. J. & Wilson, W. R. Extravascular diffusion of tirapazamine: effect of metabolic consumption assessed using the multicellular layer model. *International Journal of Radiation Oncology* Biology* Physics* **42**, 641-649 (1998).
2. Wei, C., Srivastava, D. & Cho, K. Thermal expansion and diffusion coefficients of carbon nanotube-polymer composites. *Nano Letters* **2**, 647-650 (2002).
3. Alidori, S. *et al.* Deploying RNA and DNA with functionalized carbon nanotubes. *The Journal of Physical Chemistry C* **117**, 5982-5992 (2013).
4. Boehr, D. D., Farley, A. R., Wright, G. D. & Cox, J. R. Analysis of the π - π stacking interactions between the aminoglycoside antibiotic kinase APH (3')-IIIa and its nucleotide ligands. *Chemistry & biology* **9**, 1209-1217 (2002).
5. Volkov, A. & Coppens, P. Calculation of electrostatic interaction energies in molecular dimers from atomic multipole moments obtained by different methods of electron density partitioning. *Journal of Computational Chemistry* **25**, 921-934, doi:10.1002/jcc.20023 (2004).
6. Balagurumoorthy, P., Adelstein, S. J. & Kassis, A. I. Method to eliminate linear DNA from mixture containing nicked circular, supercoiled, and linear plasmid DNA. *Analytical biochemistry* **381**, 172-174 (2008).
7. Wong, M. H. *et al.* Lipid exchange envelope penetration (LEEP) of nanoparticles for plant engineering: A universal localization mechanism. *Nano letters* **16**, 1161-1172 (2016).